*Egypt. J. Chem.* **Vol. 64,** No. 7 pp. 3651 - 3658 (2021)

**Egyptian Journal of Chemistry**

**http://ejchem.journals.ekb.eg/**

# Structural characterization and gamma-ray shielding- parameters of some phosphate glasses containing By-Pass cement dust and barium oxide

**Ragb A. Gasser*, Osama Yassin, Sayed M. Salem**

*Physics department, Faculty of Science, Al-Azhar University, Cairo, Egypt*

**Abstract**

By-Pass Cement Dust, as an industrial cement waste, was used to prepare some gamma-ray shielding glasses aiming to protect people and environment from hazard radiations, some phosphate glasses containing different amounts of by-pass cement dust have been prepared by the melt quenching method. The selected molecular composition was [(100-x) % $P_2O_5$ - (x) % By-Pass Cement Dust (where x=30,35,…,60)] in steps of five. The obtained experimental density and molar volume values were inspected and were then compared with those obtained empirically for the close packed structure of the corresponding compounds. These comparisons evidenced the short-range order and randomness character of the studied samples. From the IR analysis, different phosphate speeches appeared in the glass networks, as well as some silicate groups appeared in the spectra of all samples due to the presence of considerable amount of $SiO_2$ in by-puss cement dust. Also, the present CaO act to increase $Q^2$ and $Q^1$ species as well as to increase the non-bridge oxygen, The tetrahedral are classified using the $Q^i$ terminology .where i represent the number of bridging oxygen's per tetrahedron It appeared also that, as by-pass cement dust was increased, the intensities of O-H and H-O-H groups decreased which indicated that CaO (the major constituent of by-pass cement dust) decreases the absorption of water and strengthening the studied samples. The suitability of such glasses to act as gamma-ray shielding materials was also examined and a correlation between the chemical composition (By-Pass Cement Dust content) and gamma-ray attenuation behavior was established.

**Keywords:** By-pass Cement Dust; Phosphate glasses; Gamma–ray attenuation parameters

## 1. Introduction

Amorphous materials and glasses appear now of interest due to their important functional applications in both science and technology [1]. Many efforts have been devoted to study either high purity glasses used for scientific purposes or glasses doped with controlled amounts of environmental wastes used for commercial applications [2-3]. It is known also that the variation of the composition of a glass network affects directly the properties of such glass [4-7]. Also, the use of different radioactive isotopes in various daily life fields is spread now, and it is known that, for different nuclear radiation sources, special shielding materials are required [8-10]. Since glasses are usually transparent and can be easily manufactured, therefore, another interesting application can be checked, which is the γ-ray attenuation coefficient of the studied glasses. From another point of view, by-bass cement dust (BCD), as an industrial waste, represents a dangerous byproduct of the cement industry. And it accumulated in huge amounts in Egypt. It causes various diseases, especially those related to human respiratory systems [11]. According to the chemical analysis, such waste consists of various oxides (mainly, CaO, $SiO_2$, $Na_2O$, $K_2O$ and $Fe_2O_3$), where all these oxides can be used for manufacturing different types of oxide glass [12,13].However, in this article, it will be tried to prepare some phosphate glasses with different additives of BCD, as high as possible, aiming to consume the waste accumulation as well as to obtain low coast glasses that can be used for different industrial and scientific applications. The prepared glasses will be thoroughly investigated from the structural and electrical properties points of view. Then their gamma-ray shielding parameters will be also studied in order to investigate whether they can be used as transparent γ-ray shields or as capsulations for the radio-active wastes before interment underground.

*Corresponding author e-mail: ragb2110@gmail.com.; (Ragab Gasser).
Receive Date: 21 September 2020, Revise Date: 07 December 2020, Accept Date: 10 March 2021
DOI: 10.21608/EJCHEM.2021.43013.2884

## 2. Experimental

BCD was supplied by Tora Cement Co., Helwan, Cairo, Egypt and it was chemically analyzed by using X-ray fluorescence (XRF) apparatus model PA Analytical Axios advanced, Netherlands. The obtained chemical composition is exhibited in Table (1).The selected glasses were prepared by weighing suitable amounts of ammonium di-hydrogen ortho-phosphate and the supplied BCD, so that when melted, they supply glasses having the following composition [(70-x) $P_2O_5$ - x BCD, where (X=30, 35,…, 60) in steps of five. The batches were ground and mixed well in an agate mortar and they were then transferred into porcelain crucibles and the crucibles were inserted into an electric muffle furnace at RT. The temperature of the furnace was raised up to 1100°C during one hour and left at this temperature for 2 hours. Melts were stirred several times during melting and were then poured between two copper plates in air. The obtained glass samples -just after solidifying- were transferred to the annealing furnace at 450°C for 2 hours and the furnace was then turned off and left to cool to RT (Room Temperature) with a cooling rate of about 1.5°C/min and take the sample (50%$P_2O_5$-50%BCD) and add BaO at the expense of $P_2O_5$ [(50-x) $P_2O_5$ - 50BCD-xBaO, where ( X =0,5,…., 20) in steps of five .XRD patterns were obtained by using Rigaku-RINT 2100, outfitted with $Cuk_\alpha$ radiation of λ= 0.1541 nm and the operating current and voltage were 300 mA and 50 KV, respectively.The experimental density ($\rho_{exp}$) was measured by applying Archimedes principle, using carbon tetra-chloride ($CCl_4$) as an immersion liquid. In such principle, a sample was weighted in air ($M_a$) and in $CCl_4$ ($M_l$), and then ($\rho_{exp}$) can be calculated by using equation (1) [14].IR spectroscopic analysis was used to obtain information about the structural groups, forming the glass network, and the IR measurements were carried out using FTIR- Berken Elmar spectrometer model RTX at RT, by using KBr disk technique, where 2 mg of the powdered sample under test was weighted and mixed well with 200 mg KBr and then was pressed to obtain disks suitable for IR measurements[15].

$$\rho_{exp} = \left[\frac{M_a}{M_a - M_l}\right] \rho_l \qquad (1)$$

where ρexp & ρl are the experimental density of a sample and the density of the liquid respectively, Ma & Ml are the masses of the sample in air and in liquid respectively The experimental molar volume values $(V_m)_{exp}$ were then calculated using equation (2),

$$(V_m)_{exp} = \frac{M_m}{\rho_{exp}} \qquad (2)$$

where $M_m$ is the main molecular weight in (g/mol) of a glass sample.The empirical density values ($\rho_{emp}$) were also calculated using the following relation [14],

$$\rho_{emp} = \sum_i \rho_i X_i \qquad (3)$$

where $\rho_i$ are the densities of the oxides forming a glass sample and $X_i$ are the mole fractions of each oxide. The empirical molar volume $(V_m)_{emp}$ values were then calculated using equation (2) with replacing $\rho_{exp}$ by $\rho_{emp}$ [14].

The gamma-ray attenuation parameters (total mass attenuation coefficient $(\mu_l/\rho)_{m\ (total)}$, half value layer (HVL) and Mean free path (MFP) of a glass sample were then calculated by applying WIN-XCOM program, based on the mixture rule [15]. Attenuation coefficients of the studied glass system were measured in narrow beam transmission geometry.

Table (1), The chemical composition of the used BCD

| Constituent | CaO | $K_2O$ | SiO | $Fe_2O_3$ | $Al_2O_3$ | MgO | $Na_2O$ | * LOI |
|---|---|---|---|---|---|---|---|---|
| Amount% | 60.6 | 10.74 | 6.96 | 3.60 | 2.36 | 1.54 | 0.03 | 16.59 |

* LOI is the loss of ignition

## 3. Results and Discussion

### 3.1. Structural Characterization

Visually, all the obtained solid samples appeared to be transparent and free of inclusions and air bubbles, that is they appeared in good and homogeneous glassy phase. But, in order to confirm the amorphous state of the studied samples, XRD analysis was applied. However, Fig. (1) shows the obtained XRD patterns of all glasses where it can be seen that all patterns exhibit no any sharp crystallization peaks, but only a hump at 2Θ between 20° & 30° degree. Therefore, these results showed that, all samples exhibit amorphous nature and short-range order character [16].

On the other hand, IR analysis was early known to be an effective tool to investigate the internal structure of various glasses and amorphous materials. Therefore, Fig. (2) shows the obtained IR spectra in the range from 400 to 4400 $cm^{-1}$ for all samples.The appeared broad bands, in all spectra refer to the

homogeneity and amorphous nature of the studied glasses. But it appeared that, the range of interest is only between 400 and 2000 $cm^{-1}$. This range was undergoing to the de-convolution program in order to inspect, as really as possible, the IR bands in these spectra. However, Fig. (3) represents the de-convoluted spectrum of the sample containing 60 mol % BCD, as representative spectrum.

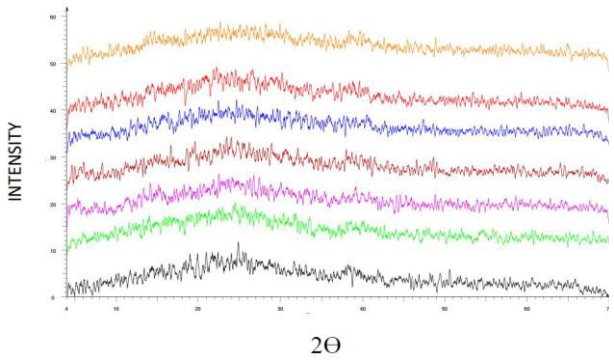


Figure 1. The obtained XRD patterns of the studied glasses

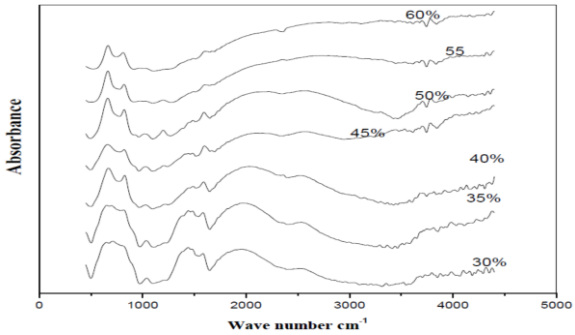


Figure 2. The obtained IR spectra of all the studied glasses

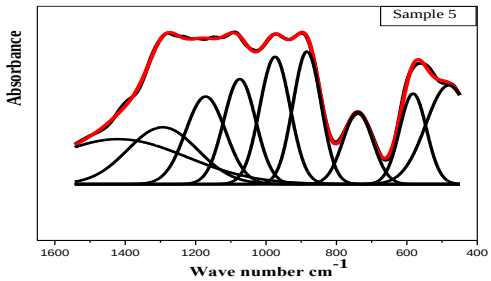


Figure 3. The de-convoluted IR spectrum of the sample containing 60 mol% BCD, as representative spectrum

The obtained real bands can be attributed to the vibration of some groups as well as some bond vibration in the glass networks and these bands can be interpreted as follows:

1. The band appeared at about 490 $cm^{-1}$ in the spectra of all samples, can be assigned to the symmetric bending vibration of Si–O–Si in $SiO_4$ tetrahedra [15].

1-The band appeared in between 550 and 580 $cm^{-1}$ can be assigned to P–O bond vibration in $PO_4$ tetrahedral [16].

2-The band appeared in the range from 735 to 760 $cm^{-1}$, in the spectra of all glasses can be attributed to the symmetric stretching vibration of P-O-P bond in $Q^1$ species [17].

3-The band appeared in between 890 and 910 $cm^{-1}$, can be assigned to the asymmetric stretching vibration of P-O-P bond in $Q^1$ species [18]. It is observed that these bonds shifted to higher frequencies, which can be attributed to some changes in phosphate chain length as well as some changes in P–O–P bond angles, since P–O–P bond angles depend on the characteristics of the metal cations in phosphate network [19].

4-The band appeared around 1055 $cm^{-1}$, can be assigned to the $PO^3$ vibration and/or the vibration of $(PO_4)^{3-}$ structural group in $Q^o$ species [20].

5-The band appeared around 1140 $cm^{-1}$ can be correlated to the vibration of two non- bridge oxygen atoms bonded to a single phosphorus atom in $PO_2$ unit (O-P-O) [21].

6-The band appeared in the range from 1215 to 1240 $cm^{-1}$, can be correlated to the symmetric stretching vibration of two non-bridge oxygen atoms bonded to a phosphorus atom in $PO_2$ unit (O-P-O) and / or the vibration O=P in $Q^2$ units [22].

7-The band appeared from 1280 to 1310 $cm^{-1}$, can be assigned to the asymmetric stretching vibration modes of non-bridging oxygen atom bonded to a phosphorus atom and/or the vibration of P=O bond in $Q^2$ species [23].

8-The band appeared in the range from 1410 to 1430 $cm^{-1}$ can be assigned to the vibration of the present molecular water or hydroxyl-related bonds [24]. However, the IR results indicated that different structural phosphate and silicate groups appeared in the glass networks, and with the gradual increase of BCD, the intensities of silicate groups vibrations increased. The introduced CaO (the major constituent in the BCD) increases the non-bridge oxygen atoms and decreases $H_2O$ and OH groups, which in turn act to strengthening the glass networks.

### 3.2. Density and Molar Volume

Both the obtained density values ($\rho_{exp}$ & $\rho_{emp}$) are plotted in Fig. (4), for comparison as a function of

BCD content. It is seen that both $\rho_{exp}$ & $\rho_{emp}$ increased gradually and linearly with the gradual increase of BCD, and the empirical density is usually higher than the corresponding experimental ones

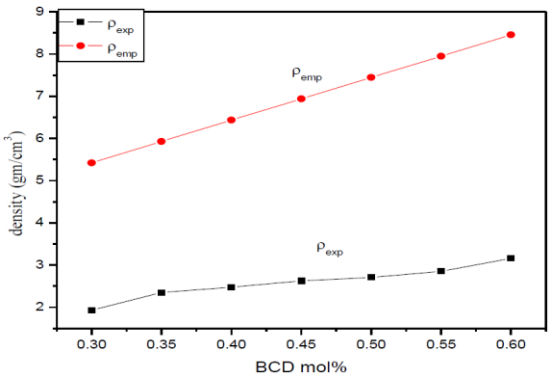


Figure 4. The variation of both density values ($\rho_{exp}$ & $\rho_{emp}$) versus BCD content

Since the molar volume is directly related to the internal spatial structure of materials, it is suitable to exhibit also the change of the molar volume as a function of BCD of the studied glasses. Both molar volume values ($V_{m\ emp}$ & $V_{m\ exp}$) are exhibited in Fig. (5), as a function of BCD.

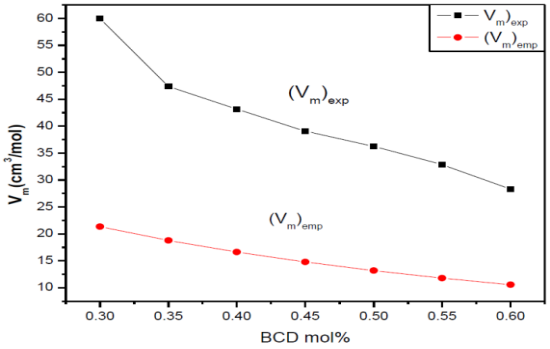


Figure 4. The variation of both density values ($\rho_{exp}$ & $\rho_{emp}$) versus BCD content

Since the molar volume is directly related to the internal spatial structure of materials, it is suitable to exhibit also the change of the molar volume as a function of BCD of the studied glasses. Both molar volume values ($V_{m\ emp}$ & $V_{m\ exp}$) are exhibited in Fig. (5), as a function of BCD.

It is observed that both values show gradual linear decrease and the empirical values are usually lower than those obtained experimentally.

The observed variations of both density and molar volume values may be due to the introduced BCD which contains various positive cations. These cations fill mostly the network vacancies, and in turn decrease the internal free volume.

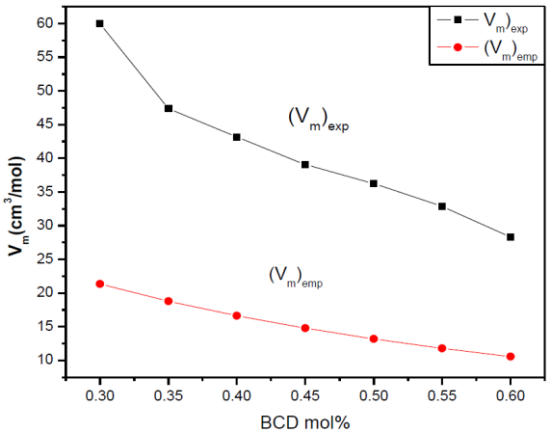


Figure 5. The variation of both molar volume values ($V_{m\ emp}$ & $V_{m\ exp}$) versus BCD content

Accordingly, the density is logically increased while the molar volume decreased. In addition, it can be stated that, the higher empirical density as well as the lower empirical molar volume in comparison to the corresponding experimental values can be taken as evidences for the amorphous nature and the short-range order character of the studied samples [7].

### 3.3. Gamma-Ray Attenuation parameters

#### 3.3.1. Historical and Theoretical

Berger and Hubbell [29] in 1987 have developed X-COM program for calculating the total mass absorption coefficients or the photon interaction cross-sections for any element, compounds or mixtures at various photon energies from 1 keV to 100 GeV. Recently, X-COM was transformed to the Windows platform by Gerward et al. [30], where it is named Win-XCom. With the development of such program, it becomes easy to calculate the total mass attenuation coefficient for different shielding materials [29, 30, 31].

However, it is preferable to check the ability of the studied glasses to act as transparent shielding materials.

The mass attenuation coefficient can be calculated experimentally by applying the following equation,

$$\mu_m = \ln (I_0 / I) / \rho_x \qquad (7)$$

Where $\rho_x$ is the measured experimental density of a material ($g/cm^3$), $I_0$ and I are the incident and transmitted intensities respectively, and x is the thickness of the absorber (cm). But the value of the total mass attenuation coefficient of a mixture or compound can be calculated applying Win-X-COM

program (based on the mixture rule) by using equation (8) [32],

$$\left(\frac{\mu}{\rho}\right)_m = \sum_i^n w_i \left(\frac{\mu}{\rho}\right)_{mi} \quad (8)$$

where $(\mu/\rho)_m$ is the total mass attenuation coefficient of a sample (mixture or compound), $(\mu/\rho)_{mi}$ is the total mass attenuation coefficient the composing elements of such sample and $w_i$ is the fractional weights of each element in the studied sample. Theoretical values for the total mass attenuation coefficient can be found in the tables prepared by Hubbell and Seltzer [31].

The linear attenuation coefficients ($\mu_L$) can be then calculated and the obtained values are correlated to the half value layer (HVL) according to equation (9),

$$HVL = 0.693/\mu_L \quad (4)$$

where HVL is the thickness of the material that decreases the intensity of the incident photon to its half value.

The Mean free path (MFP) of a gamma-ray photon ($\lambda$), was then calculated by using equation (10),

$$\lambda\ (MFP) = 1/\mu_L \quad (5)$$

where ($\lambda$) is the mean distance that the photon can travel between two successive interactions of the photon and matter.

**3.4.2. Total mass attenuation coefficient calculations**

Fig. (6) shows the variation of the calculated $\mu_m$ values for the studied glasses at different low $\gamma$-ray energies as a function of BCD content. It was found that $\mu_m$ show generally, slight linear increase with the increase of the weight fraction of BCD at the expense of $P_2O_5$. This may be due to the gradual increase in the density of the investigated glass samples. In addition, the increase in photon interaction probability at these energies leads to the decrease of gamma-rays transmission with the increase in the amount of $P_2O_5$, which indicates better shielding properties.

**3.4.3. Linear attenuation coefficient ($\mu_L$) calculations**

The linear attenuation coefficient ($\mu_L$) is the fraction attenuated from the incident photons per unit thickness of a material. It represents the fraction of photons removed from a monoenergetic beam per unit thickness of a material and it is expressed in units of 1/cm.

Fig. (7) shows the variation of linear attenuation coefficient as a function of BCD content, at different low gamma-ray energies. It appeared that, $\mu_L$ increases with the increase of BCD, which may be due to the gradual increase of density.

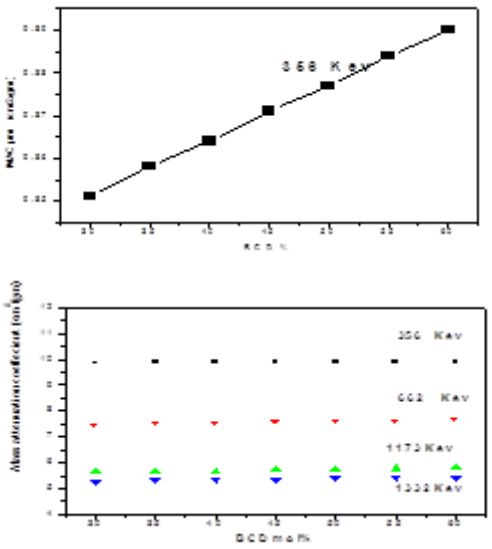


Figure 6. The variation of $\mu_m$ as a function of BCD at different low $\gamma$ – ray energies

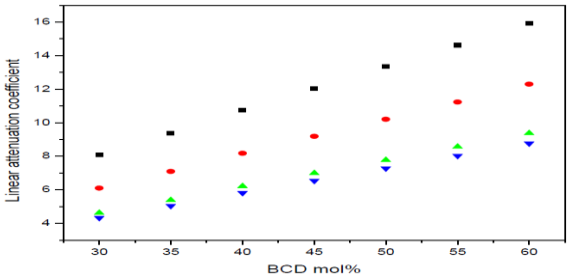


Figure 7. The variation of the $\mu_L$ as a function of BCD content at different low $\gamma$-ray energies

Table2. The variation of the Mass attenuation coefficient as a function of BCD at relatively low $\gamma$–ray energies

| Glass No | BCD mol% | Density gm/cm$^3$ | μm (cm$^2$/gm) X (10$^{-2}$) | | | |
|---|---|---|---|---|---|---|
| | | | 356 Kev | 662 Kev | 1173 Kev | 1332 Kev |
| 1 | 30 | 1.93 | 9.851 | 7.44 | 5.641 | 5.289 |
| 2 | 35 | 2.35 | 9.858 | 7.471 | 5.67 | 5.317 |
| 3 | 40 | 2.48 | 9.864 | 7.502 | 5.699 | 5.344 |
| 4 | 45 | 2.62 | 9.871 | 7.532 | 5.728 | 5.371 |
| 5 | 50 | 2.71 | 9.877 | 7.563 | 5.757 | 5.398 |
| 6 | 55 | 2.85 | 9.884 | 7.593 | 5.786 | 5.425 |
| 7 | 60 | 3.16 | 9.89 | 7.64 | 5.816 | 5.445 |

### 3.4.3. The half value layer and mean free path calculations

The HVL is the thickness of a material required to reduce the intensity of the transmitted radiation into its half value. Such value can be used to describe the effectiveness of the studied shields.

Fig. (8) shows the behavior of HVL for the studied glasses as a function of BCD, at various low gamma-ray energies. This figure indicates that HVL decreases with the increase of the weight fractions of BCD. This may be due to the gradual increase of linear attenuation coefficient and the densities of the studied glass samples.

The MFP is the average distance traveled by a moving photon between successive impacts. Such value can be used to describe the effectiveness of the studied shields. Fig. (9), shows the behavior of the MFP for the studied glasses as a function of BCD, at various low gamma-ray energies. This figure indicates that MFP decreases with the increase of the weight fractions of BCD. This may be due to the gradual increase of molar volume of the studied glass samples.

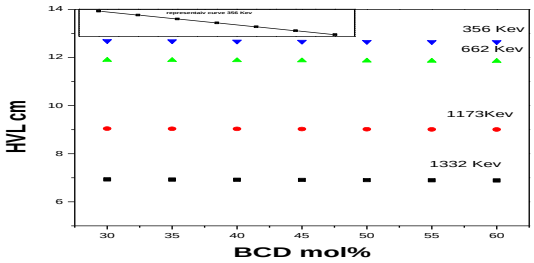


Figure 8. The variation of HVL as a function of BCD at relatively low γ – ray energies

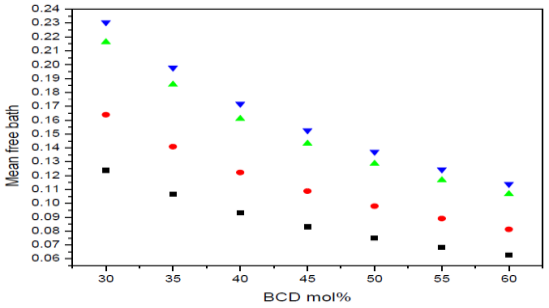


Figure 9. The variation of MFP, as a function of BCD content

Table3. The calculated HVL as a function of BCD, at relatively low gamma-ray energies

| Glass No | BCD (mol%) | Density (gm/cm$^3$) | HVL | | | |
|---|---|---|---|---|---|---|
| | | | 356 Kev | 662 Kev | 1173 Kev | 1332 Kev |
| 1 | 30 | 1.92905 | 9.999 | 7.665 | 5.828 | 5.462 |
| 2 | 35 | 2.34899 | 10.01 | 7.670 | 5.831 | 5.465 |
| 3 | 40 | 2.47639 | 10.02 | 7.675 | 5.835 | 5.469 |
| 4 | 45 | 2.62365 | 10.03 | 7.681 | 5.838 | 5.472 |
| 5 | 50 | 2.70551 | 10.04 | 7.686 | 5.842 | 5.475 |
| 6 | 55 | 2.85243 | 10.05 | 7.691 | 5.845 | 5.478 |
| 7 | 60 | 3.15972 | 10.06 | 7.696 | 5.848 | 5.481 |

### 3.4.4. The Total Mass Attenuation Coefficient of samples containing BaO

Noticing that, the studied glasses contain no any heavy metal cations (only phosphorous and BCD constituting cations), and it is supposed that, if some heavy metal cations are introduced into their network, this may improve their gamma-ray attenuation parameters. However, these parameters will be checked again when different amounts of BaO are introduced into their networks. The mass attenuation coefficients as a function of γ- ray energies for different BaO concentrations are represented in the table. (4).

It can be observed from Fig. (10) That the mass attenuation coefficient exhibits approximately gradual increase as BaO was increased, but it shows approximately gradual decrease as the γ- ray energy was increased. This behavior shows good confirmation that the introduced BaO act to increase the mass attenuation coefficient. It appeared also that the studied glass samples exhibit high shielding

efficiency at low γ- ray energies and their efficiency decreased as the γ- ray energy increased.

It can be observed from Table. (5) that the comparison between the exp. & Theo. linear attenuation coefficient of glasses containng heavy metals exhibits also approximately gradual increase as BaO was increased.

Fig. (11) show a comparison between the exp. linear attenuation coefficient of glasses containing BaO and glass without BaO. And both variations exhibits approximately gradual increase as BaO was increased.

it can be observed also that the linear attenuation coefficient of the glasses containing BaO are higher than those containing no BaO.

**Generally**, these results indicated that the studied glasses are good attenuators for gamma photons and they represent promising gamma-ray shielding materials due to their high mass attenuation coefficient and their low half value layer , especially when some BaO has introduced into their glass networks.

Table 4. The variation of the Mass attenuation coefficient as a function of BaO content at relatively low γ–ray energies.

| **BaO mol%** | **μm ($cm^2$/gm) X ($10^{-2}$)** | | | |
|---|---|---|---|---|
| | **356 Kev** | **662 Kev** | **1173 Kev** | **1332 Kev** |
| **0** | 10.1 | 7.68 | 5.83 | 5.47 |
| **5** | 10.3 | 7.69 | 5.81 | 5.44 |
| **10** | 10.5 | 7.70 | 5.78 | 5.41 |
| **15** | 10.7 | 7.71 | 5.75 | 5.39 |
| **20** | 10.9 | 7.72 | 5.72 | 5.37 |

Table (5) Shows the obtained values of the Theo. & exp. linear attenuation coefficient of glasses containing BaO

| **BaO %** | **5** | **10** | **15** | **20** |
|---|---|---|---|---|
| **Theo. μ** | **.1122** | **.1211** | **.1302** | **.1425** |
| **exp. μ** | **.1224** | **.1323** | **.1432** | **.1546** |

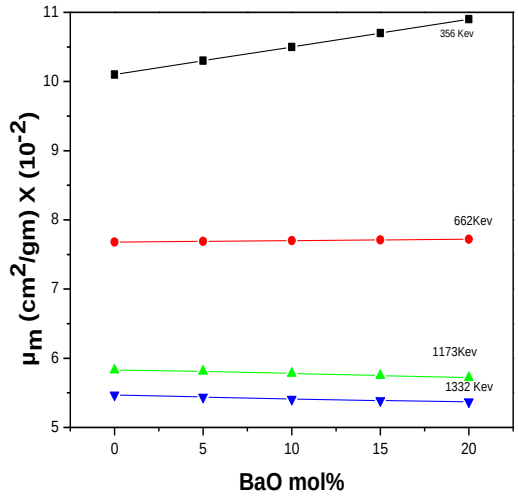


Figure 10. The variation of μm of glasses containing different concentration of BaO.

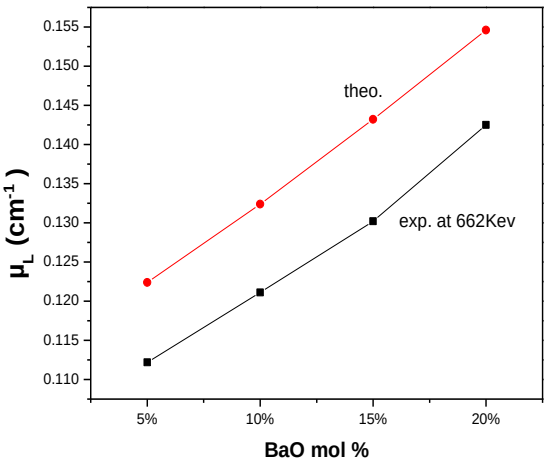


Figure 11. Comparison between exp. linear attenuation of the glasses containing different amounts of BaO content.

**CONCLUSION:**

According to the obtained results and the proposed discussion in this study, the following conclusions can be drown :

1- Some phosphate glasses with different additives of BCD (industrial iron wastes) as high as 60 mol%, can be prepared, where these glasses are environmentally friends.

2- The visual examination showed pure glassy phase of all the prepared samples, and the XRD analysis confirm their amorphous nature as well as their randomness structure.

3- The densities of the studied glasses are found to increase gradually as BCD was gradually increased.

4- The studied glasses represent good attenuators for γ –photons and promising gamma-ray shielding material due to their high mass attenuation coefficient and their low half value layer (HVL) only at low gamma-ray energies.

5- The introduced of some heavy metal cation improve all the gamma-ray shielding parameters.

**REFERENCES**


1. R. Mercier, J. P. Malugani, B. Fahys, and G. Robert, Solid State Ionics, 5 (1981) 663.
2. M. Wada, M. Mcnetrier, A. Le Vasseur and P. Hagenmuller, Mater. Res. Bull., 18 (1983) 189.
3. H. Mori, H. Matsuno and H. Sakata, J. Non-Cryst Solids, 276 (2000) 78.
4. G. D kattak, E. E. Khfaja, L. E. Wenge, D. J. Thompson, M. A. Said, A. B. Hallak and M. A. Daous, J. Non-Cryst. Solids, 194 (1990) 1.
5. A. saeed, R.M. El-Shazly, Y.H. Elbashar, and M.M. El-Okr, Radiat. Phys. Chem., 102(2014)167.
6. H.A. Saudi, A. Abd-Elalim, T.Z. Abou-Elnasr, A.G.Mostafa,Nature and Scince,13(11) (2015)139.
7. A.M. El-Khayatt, A. M.Ali and V.P. Singh, Nucl.Inst. Methods Phys. Res. (A),735 (2014) 2014.
8. S. Grandi, P. Mustarelli, A. Magistris, M. Gallorini and E. Rizzio, J. Non-Cryst. Solids, 303 (2002) 208.
9. Y. M. Mustafa and A. AL. Adway, Phys.Status Solid (A),179 (2000) 83.
10. E. Metwalli, M. Karabulut, D. L. Sideborton, M. Mrsi and R.K. Brow, J. Non-Cryst. Sollids, 344 (2004) 128.
11. A. A. Bendary, Ph. D. Thesis, Phys. Dept. Faculty of Science, AL-Azhar Univ., Egypt, (2014).
12. S. Duhan, S. Sanghi, A. Agarwal, A. Sheoran and S. Rani, Physica B, 404 (2009) 1648.
13. N.T. Sheldon Landsberger, "Measurement & Detection of Radiation" 4th edition, France (2015).
14. G. S. M. Ahmed, A. S. Mahmoud, S. M. Salem, T.Z. Abo-Elnaser .American Journal of Physics and Applications. 3(4)( 2015)112.
15. B. Qian Xiaofeng Liang, Shiyuan Yang, Shu He and Long Gao, J. Molecular Structure, 1027 (2012) 31.
16. A.M. Efimov, J. Non- Cryst. Solids, 209 (1997) 209.
17. A.G. shikerkar, J.A.E. Desa, P.S.R. Krishna and R. chitra, J. Non-Cryst. Solids, 270 (2000) 234.
18. J.C. Buyn, B.H. Kim, K.S. Hong, H.J. Jung, S. W. Lee and A. A. Lzyneev, J. Non-Cryst. Solids, 190 (1995) 288.
19. J. Koo, B.S. Bae and H.K. Na, J. Non-Cryst. Solids, 212 (1997) 193.
20. G.B. Rouse Jr., P.J. Miller and W.M. Risen, J. Non-Cryst. Solids, 28 (1978) 193.
21. C. Daynand and M.S. Graw, J. Mater. Sci., 31 (1996) 1945.
22. S.W. Martin, Eur. J. Solid Inorg. Chem., 28 (1) (1991) 163.
23. L. Baia, D. Muresan, M. Baia, J. Popp and S. Simon, Vib. Spectroscopy, 43 (2007) 313.
24. S.N. Salman and H. A. El-Batal, J. Non-Cryst. Solids, 168 (1994) 179.
25. A.M. Abdel-Ghany, A.M. Zoulfakar, T.Z. Abou-Elnasr, M.Y. Hassaan and A. G. Mostafa, American J. Phys. & Applications, 3(6) (2015) 208.
26. H.S. Chen, J. Non-Cryst. Solids, 27 (1978) 257.
27. S. Wuy, X. Wei, X. Wang, H. Yang and H. Gao, J. Mater. Sci. & Technol., 26 (5) (2010) 472.
28. J.F. Krocher, R.E. Browman "Effects of Radiation on Materials and Components", Reinhold, New York, (1984).
29. J. Berger, J.H. Hubbell, NBSIR (1987), 87.
30. L. Gerward, N. Guilbert, K.B. Jensen and H. Levring, Radiat. Phys. Chem., 60 (2001) 23.
31. J.H. Hubbell, S.M. Seltzer, NISTIR 5632 (1995).
32. A.M. Abdel-Ghany, A.M. Zoulfakar,T.Z. Abo-Elnaser, M.Y. Hassan and A.G. Moustafa, American Journal of Phys. and Applications, 3(6) (2015) 208.
33. A.M. Abdel-Ghany, M.S.S. Saad, I.I. Bashter, T.Z. Amer, S.M. Salem and A.G. Mostafa, Nature and Scince, 12(2014)162.
34. B. Qian Xiaofeng Liang, Shiyuan Yang, Shu He and Long Gao, J. Molecular Structure, 1027 (2012) 31.
35. SA Abo-El-Enein, FI El-Hosiny, SMA El-Gamal, M.S Amin, M Ramadan, J. Construction and Building Materials, 173 (2018) 687
36. M. Ramadan, M.S. Amin, Mostafa A. Sayed, "Superior physico-mechanical, Construction and Building Materials, 234(2020) 117807.
37. F.A. Selim, M.S. Amin, M. Ramadan, M.M. Hazem, Construction and Building Materials 258 (2020) 119648 .